
Band gap prediction for large organic crystal structures with machine learning

Bart Olsthoorn¹ R. Matthias Geilhufe¹ Stanislav S. Borysov² Alexander V. Balatsky¹

¹Nordita, KTH Royal Institute of Technology and Stockholm University, Sweden

²Technical University of Denmark, DTU, Denmark

Abstract

Large datasets of *ab initio* calculations have enabled many pioneering studies of machine learning applied to quantum-chemical systems. For example, machine learning models already achieve chemical accuracy on the popular QM9 dataset with small organic molecules. Here, we present a new, more challenging dataset of 12,500 large organic crystal structures and their corresponding DFT band gap, freely available at <https://omdb.diracmaterials.org/dataset>. The complexity of the organic crystals in this dataset, which have on average 85 atoms per unit cell, makes it a challenging platform for machine learning applications. We run two recent machine learning models, kernel ridge regression with the Smooth Overlap of Atomic Positions (SOAP) kernel and the deep learning model SchNet, on this new dataset and find that an ensemble of these two models reaches mean absolute error (MAE) of 0.361 eV, which corresponds to a percentage error of 12% on the average band gap of 3.03 eV. The models also provide chemical insights into the data. For example, by visualizing the SOAP kernel similarity between the crystals, different clusters of materials can be identified, such as organic metals or semiconductors. Finally, the trained models are employed to predict the band gap for 260,092 materials contained within the Crystallography Open Database (COD) and made available online so the predictions can be obtained for any arbitrary crystal structure uploaded by a user.

1 Introduction

Many properties of a crystalline material, such as electric conductivity or optical absorption spectrum, are primarily governed by its electronic structure stemming from the underlying quantum mechanical nature of the electrons. The ability to find or even design materials with target functional properties is of a key importance to sustain current technological progress. Although ever-growing computational resources and better algorithms have significantly accelerated this search, the combinatorial complexity of the problem requires development of new approaches.

In the recent decades, the amount of scientific data collected has facilitated the emergence of new data-driven approaches in the search for novel functional materials. Scientific data has been made accessible in terms of a multitude of online databases, e.g., for crystal structures [13, 14, 3], electronic structures and materials properties [19, 4, 9, 32, 31]. In contrast to pure data-mining approaches, which focus on extracting knowledge from existing datasets [5, 11, 43], machine-learning models tries to predict target properties directly, where the highly non-linear map between initial crystal structure and functional property of interest is approximated. In this context, machine learning offers an attractive framework for screening large collection of materials. Having a well-trained machine learning model at hand tremendously accelerates the identification of novel functional materials, as the prediction of the property of interest for a given crystal structure bypasses computationally expensive modelling based on *ab initio* methods.

There has been a growing interest in developing interpretable and efficient machine learning models for materials science and quantum-chemical systems [12, 39, 6, 42]. It has been reported that machine learning models have reached chemical accuracy on prediction tasks for various datasets such as the popular QM9 dataset with small organic molecules [8, 40]. Meanwhile, the Materials Project is often used to test the predictive power of models trained on mostly inorganic crystal structures [48, 40]. However, the Organic Materials Database (OMDB) provides a more challenging task: the prediction of properties for complex and lattice periodic organic crystals with an average of 85 atoms in the unit cell.

Here, an important and difficult part is to numerically represent molecules or crystal structures in a way suitable for machine learning, which has been the topic of many works [38, 16, 10, 17]. These representations (often called descriptors or features) should include the known invariances of the molecule or crystal such as translational or rotational invariance and the choice of the unit cell. Recently, there have been successful approaches that learn these representations directly by incorporating them into the model architecture [12, 39, 40].

Organic materials have attracted a lot of attention with respect to spintronic devices [44] and magnon spintronics [26], molecular qubits [25], spin-liquid physics [41], organic LEDs [29] and solar cells [1]. For the latter two, the size of the band gap, i.e., the spectral gap between the lowest unoccupied and the highest occupied electronic state, plays a significant role in their functional properties.

Given the technological importance of band gap predictions and the rapid progress in the field of machine learning based materials design, we present the newly released and freely available band gap dataset¹ (OMDB-GAP1), containing the band gaps of 12,500 three-dimensional organic molecular crystals calculated using density functional theory. We discuss the performance of recent machine learning models and crystal structure representations, namely, kernel ridge regression based on the Smooth Overlap of Atomic Positions (SOAP) kernel and the deep learning model SchNet, to provide a benchmark for the state-of-the-art given this rather small, but complex dataset. The trained models presented throughout this paper are publicly available via a web interface².

The rest of the paper is structured as follows. First, we describe the new band gap dataset (OMDB-GAP1) released for the community. Second, we introduce the applied machine learning methods and discuss their performance on this dataset. Third, we introduce the web interface and discuss predictions for available crystal structure databases. Finally, we conclude the paper with the outlook and discussion of the possible future directions.

2 Dataset

Table 1 lists the most common datasets currently used for statistical modeling of functional properties. Small organic molecules are well accounted for with the QM9 dataset [35, 34], which has enabled many pioneering studies. The new dataset introduced here, OMDB-GAP1, comes with two advantages over existing datasets. First, the dataset is consistent, i.e., all the calculations were performed the same way. Secondly, the crystal structures are, on average, much larger than other available datasets. The unit cell size ranges from 7 to 208 atoms, with an average of 85 atoms.

The dataset presented here is a subset of all the calculations contained in the OMDB, where only materials with calculated magnetic moment of less than $10^{-4} \mu_B$ are selected. In total, the OMDB-

¹<https://omdb.diracmaterials.org/dataset>

²<https://omdb.diracmaterials.org/ml>

Table 1: Comparison of the datasets currently used for property learning with OMDB-GAP1. \bar{N} indicates the average number of atoms in the molecule or unit cell. Consistency means that all data comes from identical computational framework.

Name	Size	Type	\bar{N}	Consistent
QM9	133,885	Organic molecules	18	✓
Mat. Pro.	53,340	Crystals	27 ³	✗
OMDB-GAP1	12,500	Organic crystals	85	✓

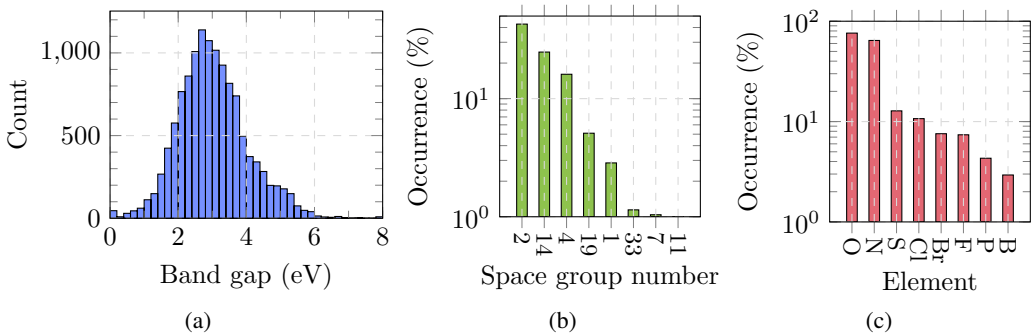


Figure 1: Descriptive statistics of the OMDb-GAP1 dataset. (a) Distribution of all 12,500 band gaps with population statistics: $\mu = 3.03$, median = 2.94, $\sigma = 1.02$. The distribution exhibits the form of the Wigner-Dyson distribution with estimated parameters: $\sim x^{4.66} e^{-0.29x^2}$ (b) The most common space groups. (c) The most common elements, excluding C and H, which occur in all the structures.

GAP1 dataset contains band gap information for 12,500 materials. The dataset comprises 65 atomic elements, with the heaviest element being Uranium, and spans 67 space groups. Figure 1b and Figure 1c show the most common space groups and atomic elements, respectively. All contained band gaps were calculated in the framework of the density functional theory by applying the Vienna ab initio simulation package VASP [22, 23], which is based on the pseudopotential projector augmented-wave method. This approach is particularly suitable to treat the sparse unit cell structures immanent to organic molecular crystals. The initial structural information of the investigated materials was taken from the Crystallography Open Database (COD) [13]. The energy cut-off was chosen to be the maximum of the specified maxima for the cut-off energies within the POTCAR files (precision flag “normal”). For the integration in \vec{k} -space a $6 \times 6 \times 6$ automatically generated, Γ -centered mesh was used.

Organics were reported to contain strongly correlated electrons as well as intermolecular van-der-Waals interactions that usually require the application of advanced exchange-correlations functionals, such as Meta-GGAs or hybrid functionals as well as van-der-Waals interactions [7, 24]. However, to obtain a statistically relevant dataset while keeping a reasonable computational demand, we chose the generalized gradient approximation according to PBE [33]. The distribution of the calculated band gaps exhibits the form of the Wigner-Dyson distribution ($\sim x^\alpha \exp(-\beta x^2)$) and is shown in Figure 1a. We argue that choosing PBE introduces a systematic error into the calculations (e.g. changing the position of the mean and the size of the variance), but does not affect the overall statistical properties of the dataset (shape of the band gap distribution). In particular the latter feature is important for the development of machine learning models, which, once they reach chemical accuracy, can be applied to an improved dataset whenever present.

Typically, the computational demand for DFT calculations tremendously increases with the number of atoms N in the unit cell. Even though implementations with $\mathcal{O}(N_{\text{atoms}})$ scaling were reported [15, 49], usual DFT codes scale with $\mathcal{O}(N_{\text{atoms}}^2 \log N_{\text{atoms}})$ up to $\mathcal{O}(N_{\text{atoms}}^3)$ [21]. However, next to the number of atoms, also other parameters like the energy cut-off for the plane-wave expansion influence the computing time. For the present dataset, the calculations took ≈ 60 core hours for each material on average, leading to a total estimate of 750k core hours for the entire dataset.

3 Models

From a machine learning point of view, band gap prediction represents a regression task, which aims to find a non-linear relation $y = f(x)$ between an input x (also called “features”) and an output y (also called “target”). The input is a molecule or crystal structure and a common strategy is to construct a descriptor x that encodes the information of the molecule or crystal structure in a fixed-size vector. Depending on the context in which the descriptors are used, certain properties such as translation, rotational, atom index invariance and differentiability are important [38, 10]. This task is difficult since equivalent crystal structures can easily lead to distinct representations, causing

inconsistent data for numerical methods. Many different descriptors have been introduced in the literature, such as the Coulomb matrix [38], Bag-of-Bonds [16], Sine Matrix [10] and MBTR [17]. An alternative strategy is to skip the intermediate step of fixed-size descriptors which often involve ad-hoc decisions and directly define the kernel between two structures as in the Smooth Overlap of Atomic Positions (SOAP) kernel, which has shown superior performance on a variety of problems [8, 18].

In this paper, two recent machine learning models will be evaluated on the new dataset: SOAP [2] and SchNet [40]. This provides an estimate of the predictive power of current models and a baseline given this dataset. In this study, the atomic numbers and positions are available, but there exist alternative approaches if only the composition of a crystal is known such as the automatically generated features from *Magpie* [45].

To train the models in this work, we use the first 10,000 structures as the training dataset and the last 2500 structures to calculate the out-of-sample predictive performance. Finally, as negative gaps are unphysical, the models' predictions are clipped to zero, i.e. $\hat{y} = \max(0, f(\mathbf{x}))$. The approximate models studied here can be used for a fast survey of desired material properties, after which traditional calculations can be used to verify the results.

3.1 Kernel Ridge Regression with SOAP

Kernel ridge regression (KRR) has been used for a variety of studies involving quantum-mechanical calculations [38, 37, 10, 8, 17, 18]. KRR corresponds to applying linear ridge regression after transforming the features $\mathbf{x} \in \mathcal{X}$ to a higher-dimensional space \mathcal{Z} . This is achieved by defining a kernel that corresponds to an inner product in \mathcal{Z} , i.e. $k(\mathbf{x}, \mathbf{x}') = \langle \phi(\mathbf{x}), \phi(\mathbf{x}') \rangle$. For a derivation of KRR see [30]. Ridge regression introduces one hyperparameter, the normalization coefficient λ , which is optimized with a grid search and using 10-fold cross validation.

The goal of the SOAP kernel is to provide a measure of similarity between two structures, i.e. a structural similarity kernel [2, 8]. In practice, this is a two-step process. First, a measure of similarity between two local environments \mathcal{X} and \mathcal{X}' is defined. Secondly, these local environment kernels are combined into a global similarity kernel. The local environment of an atom is constructed by placing a Gaussian at each neighboring atom position. The similarity (or overlap) between two environments $K(\mathcal{X}, \mathcal{X}')$ is calculated by integrating the overlap under all SO(3) rotations. For more details on SOAP see [2, 47].

The local environment kernels depend on a number of hyperparameters. The most important is the cut-off distance r_c that determines the radius of the environments considered. We set $r_c = 4 \text{ \AA}$ which marginally outperforms in a grid search $r_c = 3, 4, 5, 6 \text{ \AA}$. Additionally, the integration is in practice performed by expanding the environments in spherical and radial basis functions. This means the number of radial basis functions n and spherical basis functions l are also parameters which we set $n = 8$ and $l = 6$ as was shown sufficiently high in [2].

There are several ways local environment kernels can be combined into a global similarity kernel. Two common choices are the fast average kernel and the "regularized-entropy match" (RE-Match) kernel [8]. The fast average kernel corresponds to taking the average of all pair-wise environment kernels, whereas the RE-Match kernel is based on finding the best matches for each atomic environment [8]. However, the RE-Match scheme is prohibitively slow and memory-consuming in current implementations for the dataset that is used here, hence the fast average kernel is used⁴.

3.2 SchNet

The SchNet model is a deep learning architecture that is designed to work with both molecules and crystal structures [40]. This deep learning model is end-to-end, which means that there are no hand-crafted descriptors. The architecture is inspired by the success of convolutional neural networks applied to image and video data. However, atomic positions cannot be efficiently represented using a simple uniform grid structure as pixels in an image. Additionally, images usually have a fixed number of pixels whereas crystals can contain varying number of atoms. These issues are resolved by using weight-sharing as is common in both convolutional and recurrent neural networks (RNNs). This means the same network is used for each individual atom leading to an atom-wise contribution to the final prediction. The total number of contributions for a crystal structure varies as the total number

⁴<https://github.com/cosmo-epfl/glosim>

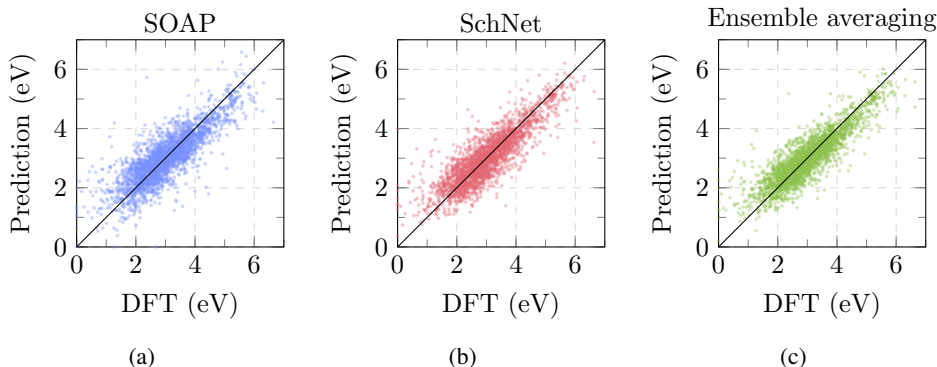


Figure 2: Band gap predictions for the 2500 test materials for the models (a) SOAP (MAE 0.418 eV), (b) SchNet (MAE 0.378 eV) and the (c) SOAP/SchNet ensemble (MAE 0.361 eV).

of atoms, and the final prediction is obtained by either averaging or summing all the contributions (referred to as pooling). Pooling maintains the atom index invariance because summing or averaging the atomic contributions is commutative. In practice, this means that SchNet decomposes a property into individual atomic contributions. For intensive properties, the mean of the atom contributions is taken, otherwise the sum is used. Besides introducing atom index invariance, it makes the model partially interpretable, since the final prediction can be explained by individual contributions.

SchNet’s architecture consists of four building blocks: atom embedding, atom-wise layers, interaction blocks and filter-generating networks. First, atoms are represented (embedded) by a vector $\mathbf{a}_Z \in \mathbb{R}^F$ depending on the proton number Z . F is the number of feature maps. Interactions with neighbouring atoms (including periodic boundary conditions) are introduced by the interaction blocks. Here, a cut-off for the environments considered is used, which we take as 5 \AA as in the original paper. The contributions by neighbouring environments in the interaction blocks are mediated by atom-wise layers and filter-generating networks. The computational details of these components are beyond the scope of this article but are available in [40]. The implementation of SchNet by the original authors is used⁵.

As in the original SchNet publication [40], the learning rate $\eta = 0.001$ is decayed exponentially, $\eta 0.96^{i/10000}$, where i is a training step. The ADAM optimizer [20] is used on mean squared error. We train SchNet for 75 epochs with a batch size of 32 and use a validation set of 1000 examples for early stopping.

Besides the standard neural network hyperparameters such as learning rate η and batch size, there are a number of parameters specific to SchNet. First of all, the cut-off radius r_c is set to 5 \AA , which was demonstrated to lead to accurate results on bulk crystal structures from the Materials Project [40]. Secondly, the dimensionality of the embeddings F is set to 64. Finally, the number of interaction blocks T is set to 6.

4 Results and Discussion

Figure 2a and Figure 2b show the out-of-sample predictions, i.e. the predictions on the 2500 test materials, for SOAP and SchNet, respectively. SchNet is more accurate (MAE 0.378 eV) than SOAP (MAE 0.418 eV) but overestimates the band gap of the metals and small-gap materials. The structural similarity kernel calculated with SOAP can be improved by an efficient implementation of the schemes alternative to the fast average kernel [8].

Table 2 summarizes the best performance of each model (after hyperparameter optimization) using the two standard metrics Mean Absolute Error (MAE) and Root Mean Square Error. The “Constant” model refers to using the mean (for RMSE) and median (for MAE) values from the training set as the most basic baselines to calculate, respectively. In machine learning, it is common practice to average

⁵<https://github.com/atomistic-machine-learning/SchNet>

the prediction of independent models to obtain an ensemble average prediction, sometimes referred to as ensemble learning [30]. Improved performance is not guaranteed, but here the average leads to the best performance of a MAE 0.361 eV and RMSE 0.482 eV, indicating that the errors of both models are slightly uncorrelated. Considering a mean band gap of 3.03 eV as shown in Figure 1a, this corresponds to a percentage error of 12%. Whether this performance is accurate enough to screen for materials and how many complementary computationally expensive DFT calculations are required depends on the application domain. For example, in the case of solar cells, the Shockley-Queisser (SQ) limit gives the maximum performance for a single p-n junction of 33.7% at a band gap of 1.34 eV, and here a MAE 0.361 eV corresponds to a performance of 28.6% (5.1% decrease) [36].

Figure 3 shows the mean absolute error (MAE) decrease with the number of training examples N on a log-log scale, revealing a roughly linear trend. For SOAP and SchNet a power law is fitted to $0.976N^{-0.093}$ and $1.884N^{-0.174}$, respectively. Extrapolation can be helpful to estimate how many materials are necessary to reach a certain level of predictive power. For example, if we aim for a MAE of 0.1 eV, which corresponds to a percentage error of 3% on the average band gap of 3.03 eV, the upper bound for SchNet is approximately 21M materials, which is far beyond the scale of available band gap data for organic molecular crystals (e.g., the COD contains crystallographic information for $\approx 325,000$ organic crystals). As this number is prohibitively large with current computational resources, it indicates the necessity for more powerful machine learning models to reach this level of accuracy. The model based on the average SOAP kernel used here is more robust (i.e. has fewer free parameters) than SchNet. Therefore, it is expected that SOAP outperforms SchNet for a small number of training examples, where SchNet is more likely to overfit, as shown in Figure 3. During training, SchNet scales linearly with the number of training examples N , whereas KRR can scale up to $\mathcal{O}(N^3)$. In practice, this means SchNet can be trained on a larger set of materials.

A measure of structural similarity $K(A, B)$ between two crystal structures A and B can be used to obtain an overview of the dataset as shown in Figure 4. The SOAP kernel used here provides a distance between two structures. The distance measure is used by a dimensionality reduction algorithm t-SNE [27] to construct a two-dimensional projection that aims to locally maintain these distances that originate from the high-dimensional space of crystal structure configurations with complex unit cells. Such a dimensionality reduction illustrates the correspondence of structural similarity and similarity in a specific property, e.g., the size of the band gap.

Figure 4 includes a selection of crystal structures visualized with the program *Mercury* [28]. The areas highlighted here show that crystal structures with similar technological applications are clustered because of characteristic structural features. For example, the structures related to chemical hydrogen storage devices appear in the vicinity of each other Figure 4a and Figure 4b. Crystal structures with a distinctive feature form an island such as the Boron-containing clusters shown in Figure 4c and Figure 4d. Similarly, pure molecular crystals appear in the region of Figure 4e and Figure 4f. The OMDB-GAP1 only includes 39 metals and the molecular metal shown in Figure 4g and structurally similar organic superconductor Figure 4h appear close to each other. Other regions of interest can be studied in the online interactive version. In general, the dimensionality-reduced visualization

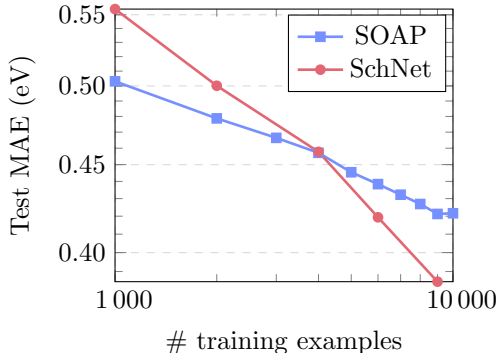


Figure 3: Benchmark of SOAP and SchNet on the OMDB band gap dataset (OMDB-GAP1). SOAP is used with an average kernel and with $r_c = 4 \text{ \AA}$, $n = 8$, $l = 6$. SchNet is used with $T = 6$, $F = 64$ and a validation set of 1000 materials is used for early stopping.

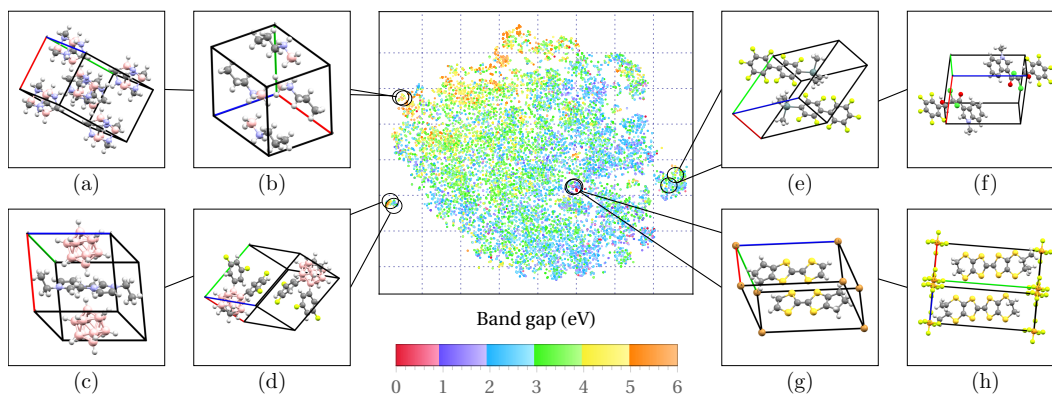


Figure 4: Dimensionality-reduced visualization of the crystal structures with t-SNE [27] with perplexity 50. The distance between two structures is determined by the average SOAP kernel ($r_c = 4 \text{ \AA}$, $n = 8$, $l = 6$). The PBE band gap is shown for each structure and regions with both similar structure and band gap are naturally appearing. A selection of crystal structures are visualized with the program *Mercury* [28]. Structures related to chemical hydrogen storage devices appear in the vicinity of (a) OMDB-ID 36754 ($C_4 H_{14} B_4 N_4$) and (b) OMDB-ID 22958 ($C_3 H_{12} B N$). Structures with a similar Boron-containing clusters form the island including (c) OMDB-ID 4085 ($C_{12} H_{34} B_{12} N_4$) and (d) OMDB-ID 26557 ($C_{14} H_{16} B_{10} F_4$). Molecular crystals are present in the region of (e) OMDB-ID 23379 ($C_{15} H_9 F_9 Sn$) and (f) OMDB-ID 4532 ($C_{18} H_{10} Cl_2 F_5 N O_2$). Molecular metal (g) OMDB-ID 16923 ($C_{18} H_{16} Br S_8$) and a structurally similar organic superconductor (h) OMDB-ID 33839 ($C_{24} H_{24} F_6 P S_{16}$) appear in the same zero band gap region. Online interactive version (with zoom) available at <https://omdb.diracmaterials.org/dataset/OMDB-GAP1/interactive>.

where the functional property (e.g. band gap) is color-coded provides an intuitive way to navigate the structure-property landscape of organic crystals.

For the SchNet model, the learned embeddings a_Z can be studied in a dimensionality reduced picture, which shows that SchNet has learned similarity between certain atom types as in the periodic table (Figure 5). Note that extracting the periodic table from machine learning models is also possible in the case of SOAP with a chemical environment kernel [46]. Alternatively, it is also possible to use only compositional information to create atom embeddings that can reconstruct the periodic table [50].

Web interface

Additionally, we launched a web interface⁶ that can predict band gap properties for a user-uploaded Crystallographic Information File (CIF) containing the crystal structure. The trained models scale differently when presented a new crystal structure. SchNet is a parametric model with a fixed number of parameters per atom that is evaluated on each site, and therefore scales linearly with the system size [40]. Kernel ridge regression, on the other hand, scales with the number of training examples N because it requires calculating the kernel between the new structure A and the reference example

⁶<https://omb.diracmaterials.org/ml>

Table 2: Summary of performance with all training examples. Constant represents a baseline by predicting the median and mean of the training examples for MAE and RMSE, respectively.

	MAE (eV)	RMSE (eV)
Constant	0.781	1.006
SOAP	0.418	0.558
SchNet	0.378	0.513
Ensemble averaging	0.361	0.482

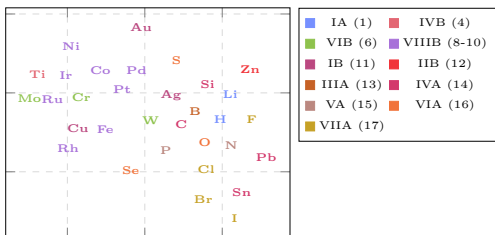


Figure 5: t-SNE (perplexity 10) of the learned embeddings \mathbf{a}_Z ($F = 64$ -dimensional) in SchNet ($T = 6, 9000$ training examples). Elements that occur in fewer than 40 materials are ignored. Groups of the periodic table (denoted by CAS numbering) can be recognized.

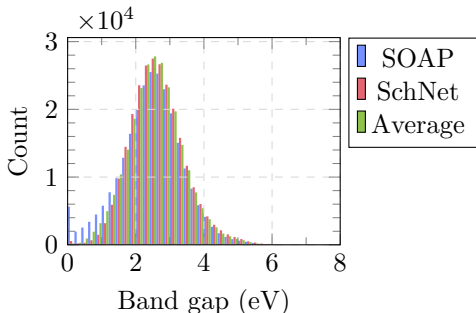


Figure 6: Distribution of 260,092 COD band gap predictions. The distribution exhibits the form of the Wigner-Dyson distribution with estimated parameters $\sim x^{4.98}e^{-0.40x^2}$, $\sim x^{5.37}e^{-0.43x^2}$ and $\sim x^{5.25}e^{-0.43x^2}$ for SOAP, SchNet and the ensemble average, respectively.

structures to make a prediction g , i.e. $g = \sum_i^N \alpha_i K(A, B_i)$, where α_i are the regression coefficients. The predictions by the trained models are executed in parallel and shown in the online interface after ≈ 10 seconds for SchNet and ≈ 1 minute for SOAP, respectively.

Large-scale material screening

The previously trained models are able to make band gap predictions for millions of organic crystal structures within hours instead of months or years that would be required by DFT calculations. As a demonstration we employ the trained models to calculate the band gap for the materials contained in the Crystallography Open Database (COD)⁷. The database contains 399,020 Crystallographic Information Files (CIF), of which 307,013 are organic (i.e. include C and H) and consist of the 65 atomic elements present in OMDB-GAP1. The COD has an average of 317 atoms in the unit cell, significantly larger than the average of 85 within our dataset. To eliminate extremely large structures we only consider structures with fewer or equal than 500 atoms in the unit cell, leading to 260,092 structures. Figure 6 shows the distribution of band gap predictions which is similar to Figure 1a. As a proof of concept, we search for predicted solar cells around the Shockley-Queisser (SQ) limit (1.34 ± 0.05) eV of the SOAP/SchNet average ensemble predictions and find 3874 candidate materials (excluding materials present in OMDB-GAP1). This represents 1.5% of the initial search space on which more accurate high throughput DFT calculations can be used for verification. Note that this search does not take the band dispersion into account and whether a band gap is direct or indirect. A more extensive study focused on organic solar cells will be the topic of future work.

5 Conclusions

We proposed a new tool to make testable predictions of the band gaps in organic materials. The band gap of a material controls a host of physical properties and hence its knowledge will be an important ingredient in the search and prediction of viable candidates for applications. We comment on the possible utility of the method e.g for a fast throughput search of organic solar cell materials. The new OMDB-GAP1 dataset introduced here contains 12,500 organic crystal structures and DFT band gaps calculated within the same computational framework. This dataset provides a benchmark for the development of more powerful statistical modelling tools. Previous datasets such as the QM9 dataset with small organic molecules have enabled many pioneering studies, and the OMDB-GAP1 dataset establishes an even more challenging benchmark. The performance of two different recent models, SOAP and SchNet, have been evaluated here, as well as an ensemble average that shows the best performance of MAE 0.361 eV. This result provides a baseline for future machine learning model development. We employed the trained models to predict the band gap for the Crystallography Open

⁷The COD predictions are available to download from <https://omdb.diracmaterials.org/dataset>

Database (COD). Additionally, a web interface is made available where a user can obtain a prediction for any crystal structure of interest.

6 Acknowledgement

We are grateful for support from the Swedish Research Council Grant No. 638-2013-9243, the Knut and Alice Wallenberg Foundation, and the European Research Council under the European Union's Seventh Framework Program (FP/2207-2013)/ERC Grant Agreement No. DM-321031 and the Marie Skłodowska-Curie grant agreement no. 713683 (COFUNDfellowsDTU). The authors acknowledge computational resources from the Swedish National Infrastructure for Computing (SNIC) at the Center for High Performance Computing (PDC) and the High Performance Computing Center North (HPC2N) and the Uppsala Multidisciplinary Center for Advanced Computational Science (UPPMAX).

References

- [1] D. Baran, R. S. Ashraf, D. A. Hanifi, M. Abdelsamie, N. Gasparini, J. A. Röhr, S. Holliday, A. Wadsworth, S. Lockett, M. Neophytou, et al. Reducing the efficiency–stability–cost gap of organic photovoltaics with highly efficient and stable small molecule acceptor ternary solar cells. *Nature materials*, 16(3):363, 2017.
- [2] A. P. Bartók, R. Kondor, and G. Csányi. On representing chemical environments. *Phys. Rev. B*, 87:184115, May 2013.
- [3] G. Bergerhoff, I. Brown, F. Allen, et al. Crystallographic databases. *International Union of Crystallography, Chester*, 360:77–95, 1987.
- [4] S. S. Borysov, R. M. Geilhufe, and A. V. Balatsky. Organic materials database: An open-access online database for data mining. *PLOS ONE*, 12(2):e0171501, feb 2017.
- [5] S. S. Borysov, B. Olsthoorn, M. B. Gedik, R. M. Geilhufe, and A. V. Balatsky. Online search tool for graphical patterns in electronic band structures. *Npj Computational Materials*, 4(1):46, 2018.
- [6] F. Brockherde, L. Vogt, L. Li, M. E. Tuckerman, K. Burke, and K.-R. Müller. Bypassing the kohn-sham equations with machine learning. *Nature Communications*, 8(1), oct 2017.
- [7] H. K. Buchholz and M. Stein. Accurate lattice energies of organic molecular crystals from periodic turbomole calculations. *Journal of Computational Chemistry*, 39(19):1335–1343, mar 2018.
- [8] S. De, A. P. Bartók, G. Csányi, and M. Ceriotti. Comparing molecules and solids across structural and alchemical space. *Physical Chemistry Chemical Physics*, 18(20):13754–13769, 2016.
- [9] C. Draxl and M. Scheffler. Nomad: The fair concept for big-data-driven materials science. *arXiv preprint arXiv:1805.05039*, 2018.
- [10] F. Faber, A. Lindmaa, O. Anatole von Lilienfeld, and R. Armiento. Crystal Structure Representations for Machine Learning Models of Formation Energies. *ArXiv e-prints*, Mar. 2015.
- [11] R. M. Geilhufe, S. S. Borysov, D. Kalpakchi, and A. V. Balatsky. Towards novel organic high- T_c superconductors: Data mining using density of states similarity search. *Physical Review Materials*, 2(2):024802, 2018.
- [12] J. Gilmer, S. S. Schoenholz, P. F. Riley, O. Vinyals, and G. E. Dahl. Neural message passing for quantum chemistry. In D. Precup and Y. W. Teh, editors, *Proceedings of the 34th International Conference on Machine Learning*, volume 70 of *Proceedings of Machine Learning Research*, pages 1263–1272, International Convention Centre, Sydney, Australia, 06–11 Aug 2017. PMLR.
- [13] S. Gražulis, D. Chateigner, R. T. Downs, A. F. T. Yokochi, M. Quirós, L. Lutterotti, E. Manakova, J. Butkus, P. Moeck, and A. Le Bail. Crystallography Open Database – an open-access collection of crystal structures. *Journal of Applied Crystallography*, 42(4):726–729, Aug 2009.
- [14] C. R. Groom, I. J. Bruno, M. P. Lightfoot, and S. C. Ward. The Cambridge Structural Database. *Acta Crystallographica Section B*, 72(2):171–179, Apr 2016.
- [15] C. F. Guerra, J. Snijders, G. t. te Velde, and E. Baerends. Towards an order- n dft method. *Theoretical Chemistry Accounts*, 99(6):391–403, 1998.
- [16] K. Hansen, F. Biegler, R. Ramakrishnan, W. Pronobis, O. A. von Lilienfeld, K.-R. Müller, and A. Tkatchenko. Machine learning predictions of molecular properties: Accurate many-body potentials and nonlocality in chemical space. *The Journal of Physical Chemistry Letters*, 6(12):2326–2331, jun 2015.
- [17] H. Huo and M. Rupp. Unified representation of molecules and crystals for machine learning, 2017.
- [18] M. O. J. Jäger, E. V. Morooka, F. F. Canova, L. Himanen, and A. S. Foster. Machine learning hydrogen adsorption on nanoclusters through structural descriptors. *npj Computational Materials*, 4(1), jul 2018.
- [19] A. Jain, S. P. Ong, G. Hautier, W. Chen, W. D. Richards, S. Dacek, S. Cholia, D. Gunter, D. Skinner, G. Ceder, and K. a. Persson. The Materials Project: A materials genome approach to accelerating materials innovation. *APL Materials*, 1(1):011002, 2013.
- [20] D. P. Kingma and J. Ba. Adam: A method for stochastic optimization. *CoRR*, abs/1412.6980, 2014.

- [21] G. Kresse and J. Furthmüller. Efficiency of ab-initio total energy calculations for metals and semiconductors using a plane-wave basis set. *Computational materials science*, 6(1):15–50, 1996.
- [22] G. Kresse and J. Furthmüller. Efficient iterative schemes for ab initio total-energy calculations using a plane-wave basis set. *Physical Review B*, 54(16):11169, 1996.
- [23] G. Kresse and D. Joubert. From ultrasoft pseudopotentials to the projector augmented-wave method. *Physical Review B*, 59(3):1758, 1999.
- [24] L. Kronik and A. Tkatchenko. Understanding molecular crystals with dispersion-inclusive density functional theory: pairwise corrections and beyond. *Accounts of chemical research*, 47(11):3208–3216, 2014.
- [25] J. Lehmann, A. Gaita-Arino, E. Coronado, and D. Loss. Spin qubits with electrically gated polyoxometalate molecules. *Nature Nanotechnology*, 2(5):312, 2007.
- [26] H. Liu, C. Zhang, H. Malissa, M. Groesbeck, M. Kavand, R. McLaughlin, S. Jamali, J. Hao, D. Sun, R. A. Davidson, et al. Organic-based magnon spintronics. *Nature materials*, page 1, 2018.
- [27] L. v. d. Maaten and G. Hinton. Visualizing data using t-sne. *Journal of machine learning research*, 9(Nov):2579–2605, 2008.
- [28] C. F. Macrae, P. R. Edgington, P. McCabe, E. Pidcock, G. P. Shields, R. Taylor, M. Towler, and J. van de Streek. Mercury: visualization and analysis of crystal structures. *Journal of Applied Crystallography*, 39(3):453–457, Jun 2006.
- [29] M. Mesta, M. Carvelli, R. J. De Vries, H. Van Eersel, J. J. Van Der Holst, M. Schober, M. Furno, B. Lüssem, K. Leo, P. Loeb, et al. Molecular-scale simulation of electroluminescence in a multilayer white organic light-emitting diode. *Nature materials*, 12(7):652, 2013.
- [30] K. Murphy. *Machine learning : a probabilistic perspective*. MIT Press, Cambridge, Mass, 2012.
- [31] M. Nakata and T. Shimazaki. Pubchemqc project: A large-scale first-principles electronic structure database for data-driven chemistry. *Journal of chemical information and modeling*, 57(6):1300–1308, 2017.
- [32] C. Ortiz, O. Eriksson, and M. Klintonberg. Data mining and accelerated electronic structure theory as a tool in the search for new functional materials. *Computational Materials Science*, 44(4):1042 – 1049, 2009.
- [33] J. P. Perdew, K. Burke, and M. Ernzerhof. Generalized gradient approximation made simple. *Physical review letters*, 77(18):3865, 1996.
- [34] R. Ramakrishnan, P. O. Dral, M. Rupp, and O. A. von Lilienfeld. Quantum chemistry structures and properties of 134 kilo molecules. *Scientific Data*, 1, 2014.
- [35] L. Ruddigkeit, R. van Deursen, L. C. Blum, and J.-L. Reymond. Enumeration of 166 billion organic small molecules in the chemical universe database GDB-17. *Journal of Chemical Information and Modeling*, 52(11):2864–2875, nov 2012.
- [36] S. Rühle. Tabulated values of the shockley–queisser limit for single junction solar cells. *Solar Energy*, 130:139–147, jun 2016.
- [37] M. Rupp. Machine learning for quantum mechanics in a nutshell. *International Journal of Quantum Chemistry*, 115(16):1058–1073, jul 2015.
- [38] M. Rupp, A. Tkatchenko, K.-R. Müller, and O. A. von Lilienfeld. Fast and accurate modeling of molecular atomization energies with machine learning. *Phys. Rev. Lett.*, 108:058301, Jan 2012.
- [39] K. T. Schütt, F. Arbabzadah, S. Chmiela, K. R. Müller, and A. Tkatchenko. Quantum-chemical insights from deep tensor neural networks. *Nature Communications*, 8:13890, jan 2017.
- [40] K. T. Schütt, H. E. Sauceda, P.-J. Kindermans, A. Tkatchenko, and K.-R. Müller. SchNet – a deep learning architecture for molecules and materials. *The Journal of Chemical Physics*, 148(24):241722, jun 2018.
- [41] Y. Shimizu, K. Miyagawa, K. Kanoda, M. Maesato, and G. Saito. Spin liquid state in an organic mott insulator with a triangular lattice. *Phys. Rev. Lett.*, 91:107001, Sep 2003.
- [42] V. Stanev, C. Oses, A. G. Kusne, E. Rodriguez, J. Paglione, S. Curtarolo, and I. Takeuchi. Machine learning modeling of superconducting critical temperature. *npj Computational Materials*, 4(1), jun 2018.
- [43] S. K. Suram, J. A. Haber, J. Jin, and J. M. Gregoire. Generating information-rich high-throughput experimental materials genomes using functional clustering via multitree genetic programming and information theory. *ACS Combinatorial Science*, 17(4):224–233, mar 2015.
- [44] V. Vardeny. Spintronics: Organics strike back. *Nature materials*, 8(2):91, 2009.
- [45] L. Ward, A. Agrawal, A. Choudhary, and C. Wolverton. A general-purpose machine learning framework for predicting properties of inorganic materials. *npj Computational Materials*, 2(1), aug 2016.
- [46] M. J. Willatt, F. Musil, and M. Ceriotti. A Data-Driven Construction of the Periodic Table of the Elements. *ArXiv e-prints*, June 2018.
- [47] M. J. Willatt, F. Musil, and M. Ceriotti. Theory and Practice of Atom-Density Representations for Machine Learning. *ArXiv e-prints*, July 2018.
- [48] T. Xie and J. C. Grossman. Crystal graph convolutional neural networks for an accurate and interpretable prediction of material properties. *Phys. Rev. Lett.*, 120:145301, Apr 2018.
- [49] R. Zeller. Towards a linear-scaling algorithm for electronic structure calculations with the tight-binding korringa–kohn–rostocker green function method. *Journal of Physics: Condensed Matter*, 20(29):294215, 2008.
- [50] Q. Zhou, P. Tang, S. Liu, J. Pan, Q. Yan, and S.-C. Zhang. Learning atoms for materials discovery. *Proceedings of the National Academy of Sciences*, 2018.